Journal of Molecular Liquids 340 (2021) 117230

Contents lists available at ScienceDirect

Journal of Molecular Liquids

journal homepage: www.elsevier.com/locate/molliq

Synthesis and characterization of a lipase-friendly DES based on cholinium dihydrogen phosphate

María S. Álvarez [a,b,*], María A. Longo [a,b], Francisco J. Deive [a,b], Ana Rodríguez [a,*]

[a] Departamento de Ingeniería Química, Universidade de Vigo, Vigo 36310, Spain
[b] CINTECX - Universidade de Vigo, Campus As Lagoas-Marcosende, Vigo 36310, Spain

ARTICLE INFO

Article history:
Received 16 May 2021
Revised 26 July 2021
Accepted 8 August 2021
Available online 12 August 2021

Keywords:
Cholinium dihydrogen phosphate
Deep Eutectic Solvents
Physico-chemical characterization
Lipase
Ethylene glycol
Glycerol

ABSTRACT

The main objective of the present work was to synthesize and characterize three novel lipase-friendly deep eutectic solvents (DESs) using cholinium dihydrogen phosphate (N_{1112OH}DHP) as hydrogen bond acceptor and ethylene glycol (EG) and/or glycerol (GL) as hydrogen bond donors in the following proportions: N_{1112OH}DHP:EG (molar ratio 1:2), N_{1112OH}DHP:GL (molar ratio 1:2) and N_{1112OH}DHP:EG:GL (molar ratio 1:1:1). FTIR, ^{1}H NMR, TGA and DSC were employed to shed light on their distinctive structural characteristics. Density, refractive index and dynamic viscosity were also measured at different temperatures, and the experimental data were correlated with several well-known equations. Finally, the suitability of the newly synthesized DESs to be employed in biocatalytic reactions was demonstrated by analysing the activity of a commercial enzyme (*Candida antarctica* lipase B) after being in contact with them.

1. Introduction

The principles of Green Chemistry have furthered a revolution in the design of industrial processes, promoting the research of more environmentally friendly solvents like ionic liquids and deep eutectic solvents (DESs). The latter display lower melting points than their constituent materials (Brønsted or Lewis acids), probably due to the establishment of more complex hydrogen bonds. DESs are defined as a neoteric class of solvents sharing many of the advantages offered by ionic liquids (negligible vapour pressure, tunability and broad liquid range) and even overcoming some of their drawbacks, like their environmental persistence and toxicity [1,2]. Since the first paper tackling DES in 2001 [3] was published, a booming interest has been focused on this field [4]. Usually, they are the result of complexating quaternary ammonium or phosphonium salts (hydrogen bond acceptor, HBA) and metal chlorides (Type I), metal chloride hydrates (Type II), or organic molecular components like amide, carboxylic acids or polyols (Type III) as hydrogen bond donors (HBD). There are two new types of DESs, like those composed of metal chloride hydrate and HBDs (Type IV) and non-ionic, molecular HBAs and HBDs (Type V) [5]. The hydrophilic or hydrophobic nature of their constituents allows designing DESs for a wide spectrum of applications.

The absence of costly purification stages and the low toxicity for the majority of DESs have prompted their use in an array of sectors like electrochemistry [6], metallurgy [7], liquid–liquid extraction [8], absorption [9], biotechnology [10], nanotechnology [11] and biocatalysis [12-16]. More specifically, the biocompatibility of many ammonium salts like cholinium-type [17] is an asset to successfully propose this kind of ammonium-derived DESs for enzyme-catalyzed reactions and extraction of biocatalysts from culture broths. For instance, the suitability of cholinium-based ionic liquids regarding conventional molten salts has been demonstrated in a diversity of studies of our research group [18,19], and they have already been employed for the extraction of enzymes like pectinases or lipases [20,21]. Therefore, the effect of cholinium-based DES on the activity of enzymes must be investigated prior to proposing their use in biocatalytic reactions.

In this work, three novel DESs based on cholinium dihydrogen phosphate were synthesized with ethylene glycol and/or glycerol as HBDs. Different techniques like FTIR, ^{1}H NMR, TGA and DSC were employed to spectroscopically and thermally characterize the synthesized compounds. Furthermore, density, refractive index and dynamic viscosity were measured at different temperatures and atmospheric pressure, as this physico-chemical characterization is indispensable prior to proposing these DESs for future applications. The experimental data were correlated with several

* Corresponding authors.
E-mail addresses: msaa@uvigo.es (M.S. Álvarez), aroguez@uvigo.es (A. Rodríguez).

https://doi.org/10.1016/j.molliq.2021.117230
0167-7322/

empirical equations, and the effect of these solvents on the biocatalytic performance of a model lipase obtained from the yeast *Candida antarctica* was finally ascertained.

2. Materials and methods

2.1. Materials

The ionic liquid cholinium dihydrogen phosphate, N_{1112OH}DHP (CAS 83846–92-8, mass fraction purity > 0.98) was acquired from IoLiTec and moisture and traces of solvents were removed by treating it at 0.2 Pa and 50 °C before use. Choline chloride (CAS 67–48-1, mass fraction purity > 0.98), ethylene glycol (EG) (CAS 107–21-1, mass fraction purity > 0.99) and glycerol (GL) (CAS 56–81-5, mass fraction purity > 0.99) were also purchased from Sigma-Aldrich. Their water mass fraction content was calculated to be less than 0.001 (w/w) by Karl-Fisher titration. *Candida antarctica* lipase B (CaLB) was kindly donated by Novozymes.

2.2. Dess preparation

The amount of HBA ($N_{11112OH}$DHP) and HBD (EG and/or GL) were determined using a Sartorius Cubis MSA balance (125P-100-DA, ± 10^{-5} g), and three different DESs were prepared: N_{1112OH}-DHP:EG (DES1) (molar ratio 1:2), N_{1112OH}DHP:GL (DES2) (molar ratio 1:2) and N_{1112OH}DHP:EG:GL (DES3) (molar ratio 1:1:1). They were mixed in glass tubes with screw tops and heated up to 75 °C with constant magnetic agitation until a clear liquid was obtained (about one hour). Afterwards, the obtained DESs were submitted to vacuum-drying (2×10^{-1} Pa and 50 °C) for two days. Karl-Fisher titration allowed ascertaining the water mass fraction content for each DES ($6.5 \cdot 10^{-3}$ for DES1, $6.7 \cdot 10^{-3}$ for DES2 and $3.1 \cdot 10^{-3}$ for DES3). The choline-based DES (ChCl:EG, molar ratio 1:2 and water mass fraction $5.7 \cdot 10^{-3}$) was prepared as above-mentioned for ChDHP-based DESs.

2.3. Fourier transform infrared spectroscopy (FTIR)

A Thermo Scientific FTIR Nicolet™ 6700 (thermos) spectrometer equipped with ATR using a DTGS KBr detector and beamsplitter KBr was used to investigate the structure and functional groups of the DESs at room temperature. FTIR spectra were measured in the mid-infrared range (4000–400) cm^{-1} at a spectral resolution of 4 cm^{-1} and 34 scans were taken per sample. Peak height was measured using OMNIC software version 7.3 (Nicolet Instrument Corporation, USA).

2.4. Differential scanning calorimetry (DSC)

A differential scanning calorimeter (DSC Q100 TA-Instruments) coupled with a refrigerated cooling system from TA-Instruments was used to determine the different state transitions experimented by DESs and pure chemicals. Masses of samples between 4 and 6 mg were weighed and placed into hermetically-sealed aluminium pans. DSC cycles were run at atmospheric pressure as follows: samples were introduced at 25 °C, cooled from 25 °C to −80 °C at 10 °C·min^{-1}, maintained at −80 °C during 30 s and heated from −80 °C to 250 °C at 10 °C·min^{-1}. The cell was purged with nitrogen gas (flow rate 50 mL·min^{-1}) and an empty sample pan was set as the reference. All data were analysed using the Universal Analysis Software by TA Instruments. Calibrations were carried out using an indium standard (with a melting temperature of 156.59 °C, and specific enthalpy of melting of 28.7 J·g^{-1}).

2.5. Thermogravimetric analysis (TGA)

The thermal stabilities of DESs and their pure components were determined by thermogravimetric analysis (TGA) under nitrogen atmosphere using a TG/DTA-DSC Setsys evolution 1750 instrument. In brief, about 15–30 mg of DES were introduced in a platinum pan and a dynamic mode was used to determine the onset decomposition temperatures (from 20 °C to 800 °C at 10 °C·min^{-1}). Finally, a purge with dry air atmosphere from 800 °C to 900 °C (10 °C·min^{-1}) was applied. A simultaneous TGA DSC Thermal Analyzer (Setaram) was used for thermograms determination.

2.6. Nuclear magnetic resonance (^1H NMR)

^1H NMR spectra were recorded at 25 °C on a Bruker AVANCE spectrometer operating at 400 MHz. D_2O was used as a solvent and the chemical shifts were referenced to it as external standard. The spectra processing was performed with MestRe-C 4.7.0.0 software.

2.7. Physical properties determination

Densities and viscosities were determined from 25 to 70 °C and at atmospheric pressure, with a temperature precision 0.01 °C. Density (vibrating tube) data were ascertained in an Anton Paar DSA 5000 M. Dynamic viscosity was determined in a falling ball automated viscometer LOVIS 2000 M/ME using a capillary with a diameter of 2.5 mm (dynamic viscosity in extended range = 12–1 0000 mPa·s) and a standard APN-100 to carry out the calibration in the above-mentioned temperature range. Triply distilled water and dry air were employed as standards prior to the measurement of each set of samples. The combined expanded uncertainties for density and viscosity (level of confidence = 0.95, k = 2) were $U_c(\rho) = 5 \cdot 10^{-4}$ g·cm^{-3} and $Uc(\eta)$ = 1.1 mPa·s, respectively.

An ABBEMAT-WR Dr. Kernchen refractometer was employed to determine the refractive index data, in the above cited range of temperature, after calibration with tetrachloroethylene and Millipore quality water. The combined expanded uncertainty (level of confidence = 0.95, k = 2) for the measurements was calculated to be $U_c(n_D) = 4 \cdot 10^{-5}$.

2.8. Lipolytic activity in the presence of DES and standard assay

Lipolytic activity of CALB was determined after one hour in the presence of pure and aqueous solutions of DESs (2 M and 1.5 M) at 40 °C at initial activity values of 4319 U/L. The assay to quantify lipolytic activity was carried out by monitoring the hydrolysis of *p*-nitrophenyl laurate, through UV spectrophotometry (Unicam Helios β, Thermo Electron Corp). In brief, the substrate was dissolved in ethanol (2.5 mM) and 100 μL of this solution was mixed with 800 μL of 50 mM Tris-HCl buffer (pH 8 at 40 °C) containing 20 mM $CaCl_2$. 100 μL of sample were added to this mixture and 20 min of reaction time at 40 °C were allowed prior to the addition of 250 μL of 1 M Na_2CO_3 solution and maintaining the samples in an ice batch. The sample was centrifuged at 10000 rpm to remove the precipitate and the absorbance was determined at 400 nm to quantify the release of *p*-nitrophenol. One activity unit is the amount of enzyme generating 1 μmol of *p*-nitrophenol per minute under standard assay conditions; activity was expressed in U/L. The results obtained are the mean of three replicates and the standard deviations were calculated and presented in the figures.

3. Results and discussion

3.1. Dess characterization

3.1.1. FTIR and ^{1}H NMR

FTIR was employed to analyse the presence of specific functional groups that may be the rationale to explain the formation of DES from $N_{11112OH}$DHP and EG and/or GL. The spectra obtained can be visualized in Fig. 1 (DES1, DES2 and DES3) and Fig. S1 (individual pure components). Additionally, the most remarkable vibrational bands are summarized in Table 1.

The analysis of the FTIR spectra of the individual compounds (Fig. S1) reveals the existence of a broad band corresponding to O-H stretching bond (3000–3600 cm^{-1}) [22,23], which is very remarkable in the case of ethylene glycol and glycerol, due to the presence of a greater number of –OH per molecule than in the case of N_{1112OH}DHP. Moreover, the glycerol-based DES contains a higher number of OH per molecule than ethylene glycol, as demonstrated by its broader band at 3250 cm^{-1}. In addition, pure ethylene glycol (Fig. S1B) and glycerol (Fig. S1C) have significant peaks at wavenumbers of 560–600 cm^{-1} (C-OH wagging bending), 860 cm^{-1} (OH wagging bending) 1032 cm^{-1} (C-O stretching), 1454 cm^{-1} (CH_2 bending) and 2873–2937 cm^{-1} (CH_2 stretching), respectively. These vibrational bands were observed in all FTIR spectra of the synthesized DESs and the results are in agreement with previous reports where ethylene glycol and glycerol play the role of HBDs [24,25].

For evaluating the HBA contribution, the IR spectrum of cholinium salt shows characteristic vibrational bands assigned to (C–H) bending vibration of $(CH_3)_3N^+$ (1490 cm^{-1}), CH_2 bending (1457 cm^{-1}), N-H stretching (1209 cm^{-1}), CH_2CH_2-O stretching (1122 cm^{-1}), C-C stretching (958 cm^{-1}) and C-N^+ symmetric stretching (865 cm^{-1}) [26,27]. Further, the symmetric stretching of dihydrogen phosphate is located at 1075, 950 and 560 cm^{-1} [28].

Several vibrational bands were compared with pure compounds in order to assess the IR spectrum of the novel DESs. In the low wavenumber range, it is worth mentioning the C-OH and OH wagging vibrations at 503 and 676 cm^{-1}, respectively, followed by C-N^+ symmetric stretching at 860 cm^{-1}, C-C stretching (948 cm^{-1}) CH_2CH_2-O stretching (1082 cm^{-1}) and $(CH_3)_3N^+$ bending vibration (1380 cm^{-1}). It is noticeable that bands corresponding to the stretching of these functional groups have been downshifted, in line with previous results [25,27,29]. Hence, the intensity and downshift of functional groups could be indicative of a large number of hydrogen bonds network formed between the DES components.

In all cases, a band associated to alkyl groups is displayed at 1485–1420 cm^{-1}. Thus, CH_2 bending adsorption is found at 1420 cm^{-1}, as this moiety is present in the three individual components, contrarily to CH_3 asymmetric band at 1478 cm^{-1} only, that is just present in the cholinium spectrum (1434 cm^{-1}). This observation could be explained by variations in the C–N bond length that reflects in the frequency of its stretching and deformation vibrations [30].

In the range of high wavenumber, the stretching vibration absorption peaks of –OH groups between 3500 and 3000 cm^{-1} are almost the same. As can be seen, the intensity of these peaks increases in the order: DES2 > DES3 > DES1. This fact may be attributed to hydrogen bonds formed between glycerol hydroxyl groups and cholinium dihydrogen phosphate (H-O. . .H and O-H. . .PO_4^{3-}), as

Table 1
Vibrational assignments of cholinium dihydrogen phosphate-based DESs.

Wavenumbers (cm^{-1})	*Assignment*
3250	OH stretching vibration
2987	C-H stretching vibration of alkylammonium cations
2935	CH_2 asymmetric stretching vibration
2877	CH_2 symmetric stretching vibration
1478	CH_3 asymmetric stretching vibration from cholinium cation
1420	CH_2 scissoring bending stretching vibration
1380	$(CH_3)_3N^+$ bending vibration
1082	CH_2CH_2-O stretching vibration
1031	C-O stretching vibration
948	C-C stretching vibration
860	C-N^+ symmetric stretching vibration
676	OH wagging bending vibration
503	C-OH wagging bending vibration

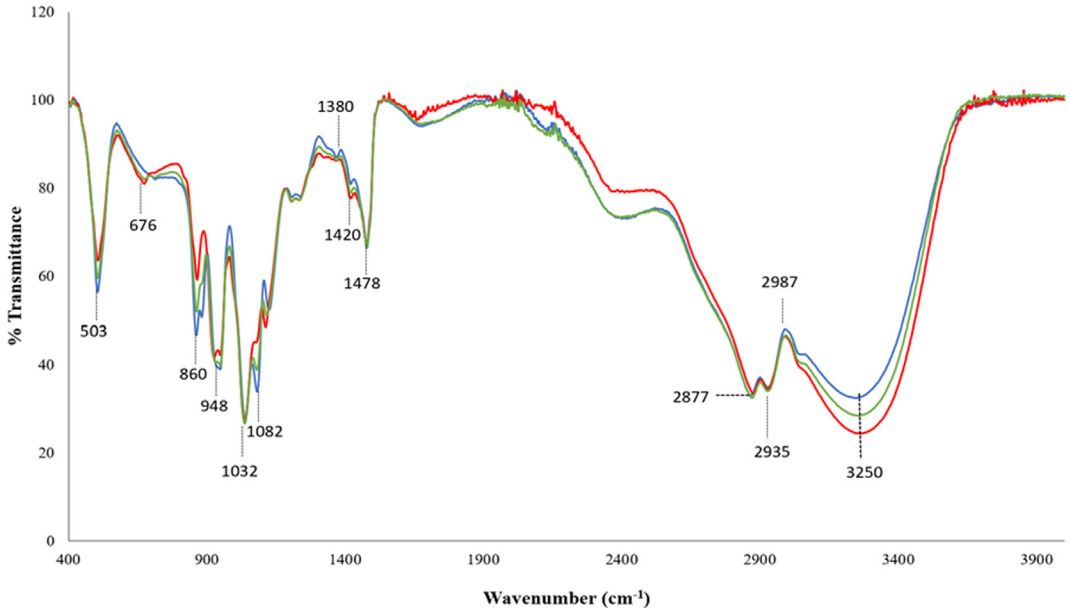

Fig. 1. Normalized ATR-FTIR spectra at 25 °C for the synthesized DESs: DES1(blue), DES2 (red) and DES3 (green).

more hydrogen bonds are formed in glycerol-based DESs. This tendency was also observed previously in cholinium-based DESs [29].

Additionally, to fully characterize the chemical structure of the selected DES, ^{1}H NMR spectroscopy was utilized. The results of ^{1}H NMR spectra of the constitutive pure substances and the synthetized DESs are shown in Fig. S2 and S3, respectively. The chemical shifts data in eutectic mixtures show a slight deviation regarding the individual compounds, which could be interpreted as a change in the chemical environment of the methylene groups after the possible formation of hydrogen bonds in DESs. The ^{1}H NMR spectra of the three DESs reveal that the signal integration is in concordance with the molar ratio of each compound, which again confirms the adequate molar composition of the proposed DES. The overlapping signals in shifts range between 3.53 and 3.70 ppm are related to the resonances of hydroxyl methylenes of the ethylene glycol (Hd) and glycerol (He) with the methylene group bound to the cholinium nitrogen (Hb), in line with previous studies performed with cholinium-based DESs. [31-33]. The residual solvent signal of D_2O at 5 ppm was not included in the graphs.

3.1.2. Thermal characterization: Thermogravimetric analysis (TGA) and differential scanning calorimetry (DSC)

Thermal stability is one of the significant aspects to take into account, as it allows defining the maximum operating temperature that DESs can withstand. Figs. 2 and 3 present the dynamic TGA/dTGA curves for the synthesized cholinium dihydrogen phosphate-based DESs and their pure constituents, respectively. As illustrated, HBD components of DESs have lower decomposition temperature compared with salt component, while glycerol and ethylene glycol-based solvents show higher and lower decomposition temperature, respectively. On the other hand, DES formed by HBDs with relatively low boiling points or poor stabilities undergo volatilization or decomposition through the weakening of the hydrogen bond interactions, thus decomposing more easily. This trend was previously observed in FTIR analysis and confirmed by preceding works [24,34,35].

For a deeper analysis of thermal stability, we will focus on the onset decomposition temperature (T_{onset}) term as it clearly reflects the maximum temperature at which DESs can maintain their liquid state without chemical decomposition [36,37]. The data obtained from the dynamic TGA/dTGA curves are compiled in Table 2. As can be observed, the values of the T_{onset} for the DESs are between those of their pure components. It is worth mentioning that depending on the eutectic mixture, more than one T_{onset} may occur. The first one indicates the decomposition temperature of HBDs which indicating the beginning of the eutectic solvent degradation and the second one is related to the breakdown temperature of salt.

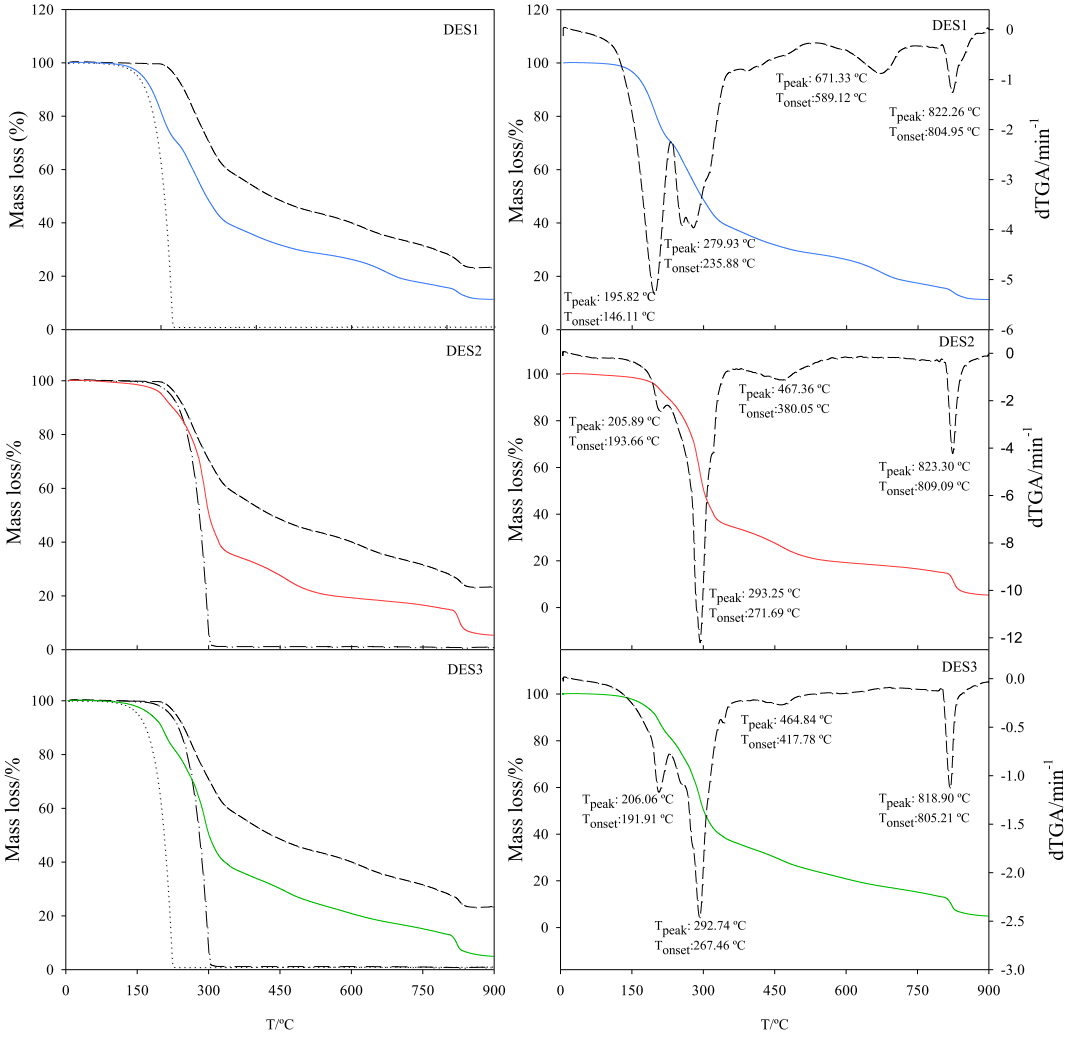

Fig. 2. On the left, TGA curves of DES with a heating rate of 10 °C·min^{-1}. Solid coloured lines represent the mass loss of DESs; (dashed) N_{1112OH}DHP, (dotted) ethylene glycol, (dash-dotted) glycerol. On the right, the TGA/dTGA curves for each DES.

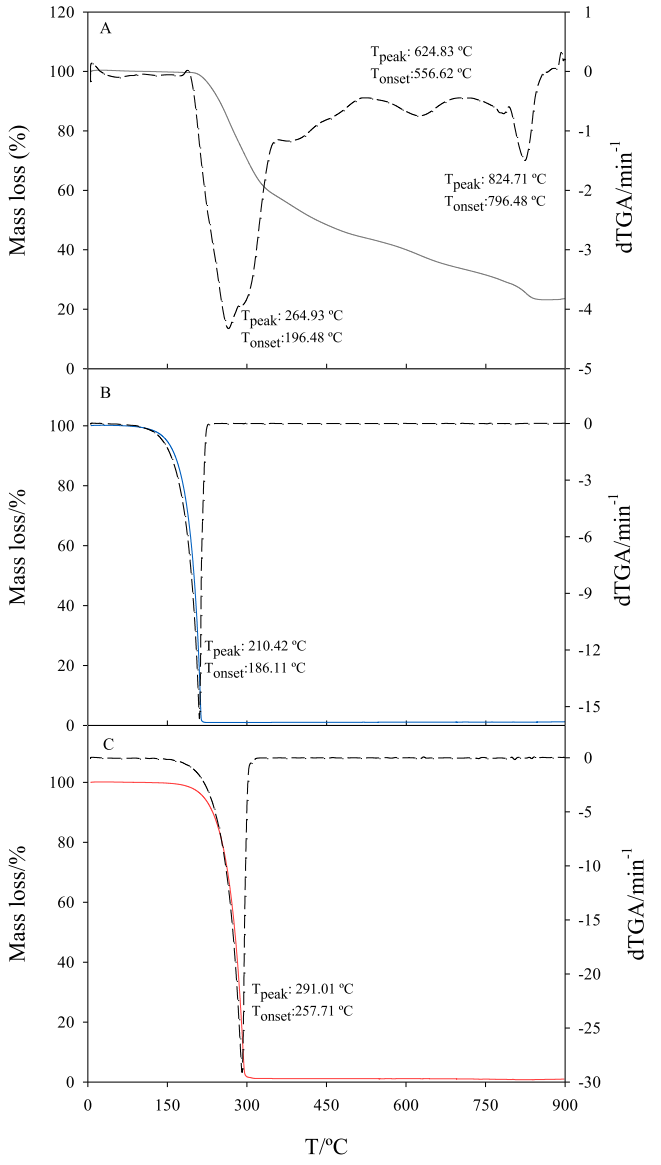

Fig. 3. TGA/dTGA curves for pure compounds at a heating rate of 10 °C·min^{-1}. (A) N_{1112OH}DHP, (B) ethylene glycol, (C) glycerol. Solid lines represent the mass loss and short dashes the first derivative of TG curves of pure compounds.

As displayed in Table 2, the first HBA T_{onset} refers to N_{1112OH}DHP melting point (196 °C), while the T_{onset} of HBDs indicates the temperature at which evaporation processes are undergone. It is also noticed that the first significant mass loss is observed at a T_{onset} over the boiling temperature for both binary (DES2) and ternary (DES3) eutectic mixtures with glycerol as HBD (271.69 °C and 267.46 °C, respectively, vs. 257.71 °C in pure glycerol), which can be attributed to glycerol vaporization. In this sense, glycerol-based DES is observed to lose 1.5 times the mass of pure glycerol at similar T_{onset} values. These outcomes may be due to the most robust hydrogen bonds network generated during the DES formation. In contrast, DES1 presents an important percentage of mass loss at T_{onset} slightly lower than the T_{onset} of pure ethylene glycol (146.11 °C in DES1 vs. 186.11 °C in pure ethylene glycol), which can be assigned to the evaporation of ethylene glycol below its boiling temperature.

The following phases of mass loss occur with the expected T_{onset} for the vaporization and decomposition processes of the pure components. These results confirm the above-mentioned stability trend (ChDHP:GL) > (ChDHP:EG:GL) > (ChDHP:EG) and are in agreement with previous reports where cholinium salts form eutectic solvents with the mentioned HBD [25,29,34]. In all cases, DESs show higher stability than pure HBD (Fig. 3). On the other hand, the chemical composition of HBA influences the thermal decomposition of DESs. Another interesting value is the T_{peak}, which can be defined as the temperature at which the sample presents the maximum degradation rate [38], (c.f. dTGA data in Fig. 2), and the values are listed in Table 2. A visual inspection of the data allows us concluding that the T_{peak} of HBDs is coincident with the estimated boiling point (290 °C and 197 °C for glycerol and ethylene glycol, respectively) [39] and T_{peak} is greater than the T_{onset}, which may lead to an estimation of the upper operation limit of these eutectic solvents.

Further, enthalpy values associated with the thermogravimetric analysis in both pure components and DES are compiled in Table 2 and the thermograms are presented in Fig. S4. It becomes clear that the thermal processes display endothermic effects except an exothermic peak associated with salt decomposition. This phenomenon is in concordance with the maximum percentage of mass loss in both DESs and N_{1112OH}DHP, which is not observed in pure HBD compounds [40].

Based on the above-mentioned, factors like the HBA and HBD chemical structures, the alkyl chain length [41], Van der Waals and hydrogen bonding interactions between the DESs components [42], electrostatic interactions and viscosity [27] play a crucial role in the thermal degradation of eutectic mixtures and will certainly impact their application potential.

In order to determine the presence of thermal transitions, the selected DESs and their pure components were characterized by DSC analysis and are presented in Fig. S5. A visual inspection of DSC plot of cholinium dihydrogen phosphate salt allows to notice an endothermic peak at 82.6 °C (47.6 J·g^{-1}), which results from a crystallographic arrangement phase transition. The same peak was observed in cholinium chloride DSC, so it seems that cholinium cation is the major contributor to this transition [43,44]. The absence of this peak in DESs is indicative that there is no excess of N_{1112OH}DHP, which may be interpreted as follows: all HBA molecules are involved in molecular interactions and the molar ratios are optimal for DES formation.

Following with DSC analysis of pure compound, ethylene glycol curve shows different peaks in the cooling and heating processes. Focusing on the cooling ramp, the melting peak (endothermic, 133.5 J·g^{-1}) at −16.48 °C and a glass transition at −64.24 °C related to the crystallization can be observed. On the other hand, the heating curve is dominated by a characteristic sharp peak at −52.81 °C, which represents a typical behaviour for glass transition where the solution could be vitrified [45,46]. No significant events were observed in glycerol sample analysed in the considered temperature range. With respect to the DSC analysis of DESs presented in this work, they do not present thermal transitions other than thermal degradation at high temperature, which can be attributed to the mass loss higher that 50% of the HBA, so it can be concluded that these eutectic solvents have been adequately synthesized.

3.2. Thermophysical properties

The complete characterization of the synthesized DESs requires the experimental determination of density, dynamic viscosity, and refractive index at temperatures comprised between 25 and 70 °C, as these properties are paramount to allow the application of these solvents. The experimental data have been ascertained and they are listed in Table 3 and presented in Figs. 4 and 5. It is clear that density decreases at greater temperature values (at constant pressure), which is attributed to the thermal expansion derived from a

Table 2
Thermogravimetric analysis of cholinium dihydrogen phosphate-based DESs at 10 °C·min^{-1} heating rate and atmospheric pressure.

dTGA results				***Heat flow (mW)***		
Compound	*T_{peak} (°C)*	*T_{onset} (°C)*	*Mass loss (%)*	*T_{peak} (°C)*	*T_{onset} (°C)*	*Enthalpy (J·g^{-1})*
N_{1112OH}DHP	54.74	13.17	0.70	99.67	81.49	53.05
	264.93	196.48	56.24	229.60	194.20	357.83
	624.83	556.62	72.03	819.81	447.71	51.31
	824.71	796.48	77.18	819.81	804.08	−621.84
EG	210.42	186.11	99.07	212.85	194.57	1061.18
GL	291.01	257.71	98.99	293.19	257.91	1117.04
DES1	195.82	146.11	30.16	202.57	161.38	116.82
	279.93	235.88	71.30	260.83	233.79	55.53
	671.33	589.12	84.35	518.64	462.13	133.98
	822.26	804.95	88.66	825.19	805.00	−329.37
DES2	66.64	39.04	0.97	nd	nd	nd
	205.89	193.66	10.63	207.97	193.48	29.78
	293.25	271.69	66.26	277.92	230.98	283.22
	467.36	380.05	85.01	496.52	358.22	534.67
	823.30	809.87	94.59	823.36	807.25	−464.89
DES3	206.06	191.91	18.87	208.00	193.75	45.88
	292.74	267.46	63.92	276.66	233.52	188.99
	464.84	417.78	86.46	489.19	410.08	265.62
	818.90	805.21	94.72	822.76	809.34	−286.07

nd: no detected

Table 3
Density, ρ, dynamic viscosity,η, and refractive index, n_D, of cholinium dihydrogen phosphate-based DESs at several temperatures and atmospheric pressure.

T/°C	ρ/(g·cm^{-3})	η/(mPa·s)	n_D
DES1			
25	1.26945	984.48	1.46907
30	1.26664	724.87	1.46802
35	1.26390	543.31	1.46697
40	1.26112	413.84	1.46590
45	1.25844	319.84	1.46485
50	1.25583	250.72	1.46377
55	1.25310	199.03	1.46272
60	1.25056	159.84	1.46170
65	1.24791	129.79	1.46065
70	1.24533	106.52	1.45956
DES2			
25	1.3181	8299.10	1.48302
30	1.31552	5361.80	1.48210
35	1.31294	3568.80	1.48121
40	1.31033	2430.90	1.48027
45	1.30772	1693.10	1.47927
50	1.30514	1204.20	1.47825
55	1.30253	873.11	1.47727
60	1.29973	644.90	1.47627
65	1.2969	484.46	1.47524
70	1.29426	369.79	1.47419
DES3			
25	1.47663	2896.40	1.47663
30	1.47563	2004.70	1.47563
35	1.47464	1416.80	1.47464
40	1.47360	1021.00	1.47360
45	1.47259	749.56	1.47259
50	1.47158	560.08	1.47158
55	1.47058	425.05	1.47058
60	1.46954	327.41	1.46954
65	1.46847	255.68	1.46847
70	1.46745	202.25	1.46745

Standard uncertainty U: U(T) = 0.01 K, combined expanded uncertainties Uc: Uc (ρ) = 5·10^{-4} g·cm^{-3}, Uc(n_D) = 4·10^{-5}; and Uc(η) = 1.1 mPa·s (level of confidence = 0.95, k = 2).

higher molecular mobility leading to higher molar volumes, in line with previous results for other DESs [47]. Analogously, as in many other solvents, including ternary DES [48], the refractive indices decreased with increasing temperature, which is a useful information regarding the electronic polarization of the DESs. Additionally, the comparison between the ternary and binary DESs confirms the above-mentioned conclusions: as glycerol-based DES bears stronger hydrogen bond interplays than the ethylene glycol counterpart, it is expected to display a lower molar volume, thus leading to greater density values, as evidenced in Fig. 4. In this sense, the resulting ternary DES density and refractive index values fall in between those of the corresponding binary DESs. Regarding viscosity, the results visualized in Fig. 5 confirm these trends, as the greater ability of glycerol to establish hydrogen bonds with the HBA involves a reduced molecular mobility and the consequent higher viscosity.

In order to shed more light on the ascertained physical properties, the following empirical equations have been employed:

$$\rho = e^{(A+B\cdot T)} \quad (1)$$

$$\rho = A\cdot e^{B\cdot T} \quad (2)$$

$$n_D = e^{(A+B\cdot T)} \quad (3)$$

$$n_D = A\cdot e^{B\cdot T} \quad (4)$$

$$\log\eta = A\cdot T - B \quad (5)$$

$$\left(\frac{1}{\eta}\right)^{\varnothing} = A + B\cdot T \quad (6)$$

where T is the temperature, and A, B and ϕ are the values of the empirical parameters, which were calculated by using the solver function in Microsoft Excel, through minimizing the standard deviation (σ) calculated with the following expression:

$$\sigma = \left(\frac{\sum_i^{n_{DAT}}\left(z_{exp} - z_{adjust}\right)^2}{n_{DAT}}\right)^{1/2} \quad (7)$$

where z_{exp} and z_{adjust} are the experimental and calculated values of the physical property, and n_{DAT} is the number of data measured. All the values of parameters and deviations obtained are included in Tables 4 and 5. The analysis of the deviations allows concluding the greater suitability of Eq. (1) and (3) to correlate

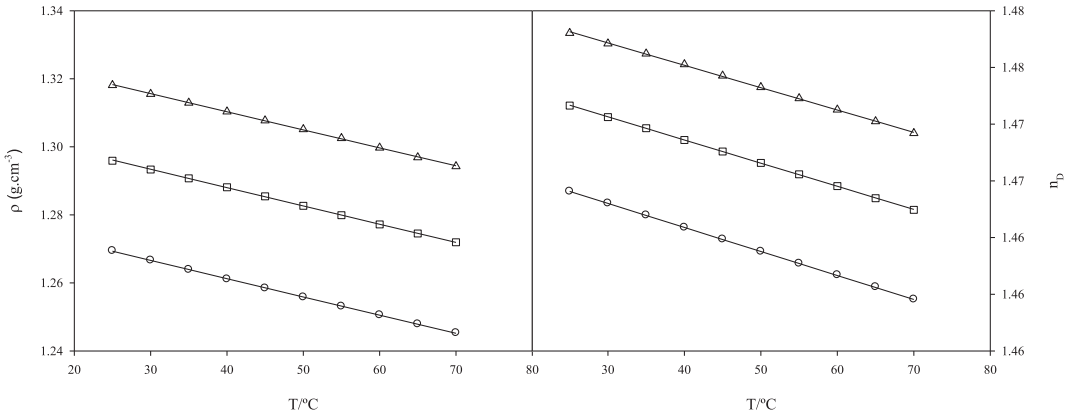

Fig. 4. Density, ρ, and refractive index, n_D, versus temperature for cholinium dihydrogen phosphate-based DES. (○) DES1, (△) DES2, (□) DES3 and solid lines represent the fitting to Eqs. (1) and (2).

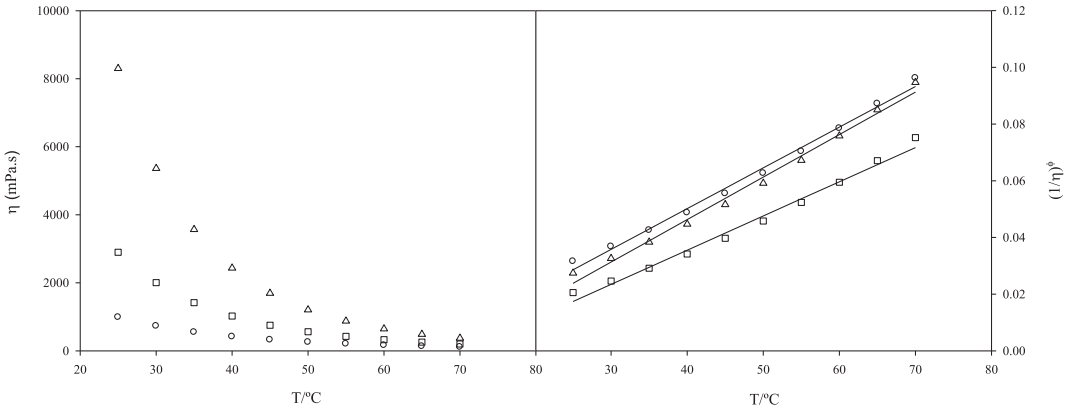

Fig. 5. Dynamic viscosity, η, (on the left) and fitting to Eq. (6) (on the right) versus temperature for cholinium dihydrogen phosphate-based DES. (○) DES1, (△) DES2, (□) DES3.

Table 4
Coefficients and standard deviations (σ) to correlate the physical properties of cholinium dihydrogen phosphate-based DESs.

	A	*B*	ϕ	σ
DES1				
ρ (g·cm^{-3})	0.24915	−0.00042		0.00009
*ρ (g·cm^{-3})	1.28312	−0.00043		0.00012
n_D	0.38825	−0.00015		0.00003
*n_D	1.47435	−0.00014		0.00002
log η(mPa·s)	−0.02138	−3.49104		0.02119
η^{ϕ} (mPa·s)	−0.00734	0.00144	0.50151	0.00176
DES2				
ρ (g·cm^{-3})	0.28649	−0.00040		0.00015
*ρ (g·cm^{-3})	1.33198	−0.00041		0.00017
n_D	0.39750	−0.00013		0.00007
*n_D	1.48808	−0.00013		0.00008
log η(mPa·s)	−0.02990	−4.61042		0.03229
η^{ϕ} (mPa·s)	−0.01367	0.00150	0.39868	0.00206
DES3				
ρ (g·cm^{-3})	0.26984	−0.00042		0.00010
*ρ (g·cm^{-3})	1.30983	−0.00041		0.00011
n_D	0.39326	−0.00014		0.00003
*n_D	1.48180	−0.00014		0.00004
log η(mPa·s)	−0.02559	−4.05609		0.02633
η^{ϕ} (mPa·s)	−0.01279	0.00121	0.48735	0.00188

Density (Eq. (1), *Eq. (2)) and refractive index (Eq. (3), *Eq. (4)); dynamic viscosities (Eq. (5); Eq. (6)); standard deviations (Eq. (7))

both the experimental densities and refractive indices in the three DESs under study, respectively. In the same line, Eq. (6) is able to fit more appropriately the experimental dynamic viscosities, as it leads to deviations one order of magnitude lower than Eq. (5). The suitable description of these models can be clearly visualized in Figs. 4 and 5.

Table 5
Fitting parameter and standard deviations (σ) to correlate the physical properties of cholinium dihydrogen phosphate-based DESs.

	k	σ
DES1		
Dale-Gladstone	0.3696	0.00020
Oster	2.2448	0.00245
Newton	0.7814	0.00651
Lorentz-Lorentz	0.2196	0.00014
Eykman	0.4882	0.00005
DES2		
Dale-Gladstone	0.3665	0.00005
Oster	2.2322	0.00151
Newton	0.8025	0.00609
Lorentz-Lorentz	0.2170	0.00022
Eykman	0.4835	0.00018
DES3		
Dale-Gladstone	0.3677	0.00010
Oster	2.2373	0.00187
Newton	0.7928	0.00630
Lorentz-Lorentz	0.2181	0.00019
Eykman	0.4855	0.00011

Analogously, the obtained density was correlated as a function of the refractive index by using the Dale-Gladstone, Oster, Newton, Lorentz-Lorenz and Eykman expressions [49]:

$$f(n_D) = \left\{ \begin{array}{c} n_D^2 - 1/n_D^2 + 2 \text{ (Lorentz - Lorenz)} \\ n_D - 1 \text{ (Dale - Gladstone)} \\ n_D^2 - 1/n_D + 0.4 \text{ (Eykman)} \\ (n_D - 1)(n_D^2 + 1)/n_D^2 \text{ (Oster)} \\ n_D \text{ (Arago - Biot)} \\ n_D^2 - 1 \text{ (Newton)} \end{array} \right\} = k\rho \quad (8)$$

where $f(n_D)$ is a function of refractive index and k is the empirical constant, which depends on the liquid and the wavelength. The values of k and deviations presented in Table 5 reveal that Dale-Gladstone and Eykman equations are those allowing a better description of the density as a function of the refractive index.

3.3. Dess and enzyme stability

Once the novel DESs have been synthesized and characterized, their biocompatibility with a model enzyme has been explored. Within the possible options, lipases are among the most relevant biocatalysts, with *Candida antarctica* lipase B (CaLB) being one of the most stable and commercialized, employed in many different fields [50]. In previous research works, we have observed that most of the ionic liquids impose deleterious effects on lipase activity [18], so the search for enzyme-friendly families has been the subject of different research works, observing the positive role of cholinium-based solvents [19].

Taking into account the benefits of DESs, it is interesting to evaluate the activity of CaLB in aqueous solutions of the synthesized DESs. One of the key aspects to be taken into account when designing a new solvent for biocatalysis purposes is the pH. In this particular case, both aqueous solutions and pure solvents display values within the range of the optimum lipase activity (data not shown), so any harmful effect due to the intrinsic pH of the solvents can be discarded. The data obtained are presented in Fig. 6, and reveal the great biocompatibility of the DESs. Relative activity levels are over 80% for both 1.5 and 2 M concentration, no matter the DES under study. Even in the pure DES, the activity attained is above 60% for both the binary and ternary DESs. The comparison of the biocatalytic performance recorded for different solvents allows concluding slightly better activity levels in the ethylene glycol-based DES, probably due to the fact that lower degree of hydrogen-bonding occurs between solvent and CaLB, that may ultimately entail no structural modifications leading to activity loss. Additionally, the evaluation of lipase stability for 24 h (c.f. Fig. S6) for both DES1 (molar ratio 1:2) and ChCl:EG (molar ratio 1:2) in 2 M solutions allowed concluding the suitability of ChDHP-based eutectic mixtures as media for biocatalysis, as they keep enzyme conformation which avoids the loss of biocatalytic potential, in a similar manner as ChCl-based DES and water. In summary, these data demonstrate the potential of these solvents to be employed in lipase extraction and in lipase-catalyzed reactions like transesterifications or interesterifications.

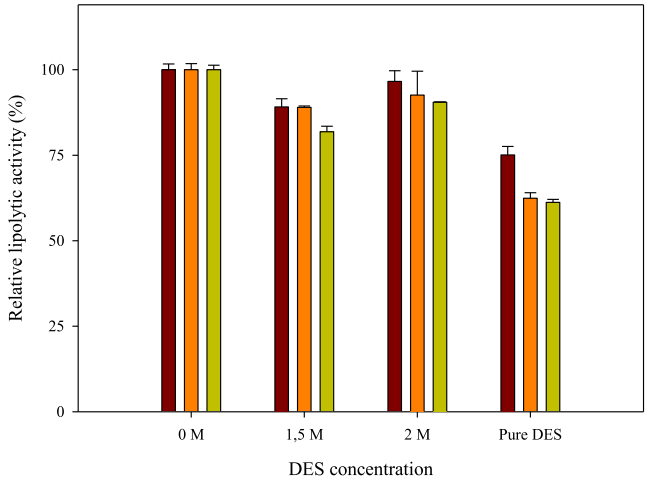

Fig. 6. Relative lipolytic activity in the presence of different DES concentration: (■) DES1, (■) DES2, (■) DES3 (100% of activity 4319 U/L).

4. Conclusions

This work has demonstrated the viability of synthesizing three novel DESs based on cholinium dihydrogen phosphate as HBA and glycerol and ethylene glycol or a mixture of both as HBD. After having structurally and thermally characterized the synthesized DESs through FTIR, ^{1}H NMR, TGA and DSC, greater hydrogen bonds interplays were concluded for glycerol-based DES. The characterization of the physical properties like density, refractive index and viscosity also confirmed this statement, as greater values were obtained for the glycerol-based solvent. Finally, the biocompatibility of the neoteric solvents was demonstrated by studying their influence on a model commercial enzyme (*Candida antarctica* lipase B), observing very high activity conservation levels even in pure DESs.

CRediT authorship contribution statement

María S. Álvarez: Conceptualization, Investigation, Formal analysis, Writing - original draft, Writing - review & editing, Funding acquisition. **María A. Longo:** Validation. **Francisco J. Deive:** Validation. **Ana Rodríguez:** Conceptualization, Writing – original draft.

Declaration of Competing Interest

The authors declare that they have no known competing financial interests or personal relationships that could have appeared to influence the work reported in this paper.

Acknowledgements

The authors thank Xunta de Galicia and ERDF for funding through a postdoctoral grant (ED481D-2019/017). The authors are grateful to the Spanish Ministry of Science, Innovation and Universities for the financial support through the project RTI2018-094702-B-I00. Authors would like to thank the use of CACTI-UVIGO and RIAIDT-USC analytical facilities.

Appendix A. Supplementary material

Supplementary data to this article can be found online at https://doi.org/10.1016/j.molliq.2021.117230.

References

[1] M. Petkovic, K.R. Seddon, L.P. Rebelo, C.S. Pereira, Chem. Soc. Rev. 40 (2011) 1383–1403.
[2] M.Q. Farooq, G.A. Odugbesi, N.M. Abbasi, J.L. Anderson, A.C.S. Sustain, Chem. Eng. 8 (2020) 18286–18296.
[3] A.P. Abbott, G. Capper, D.L. Davies, H.L. Munro, R.K. Rasheed, V. Tambyrajah, Chem. Commun. (2001) 2010–2011.
[4] E.L. Smith, A.P. Abbott, K.S. Ryder, Chem. Rev. 114 (2014) 11060–11082.
[5] B.B. Hansen, S. Spittle, B. Chen, D. Poe, Y. Zhang, J.M. Klein, A. Horton, L. Adhikari, T. Zelovich, B.W. Doherty, B. Gurkan, E.J. Maginn, A. Ragauskas, M. Dadmun, T.A. Zawodzinski, G.A. Baker, M.E. Tuckerman, R.F. Savinell, J.R. Sangoro, Chem. Rev. 121 (2021) 1232–1285.
[6] D. Lloyd, T. Vainikka, K. Kontturi, Electrochim. Acta 100 (2013) 18–23.
[7] E. Gómez, P. Cojocaru, L. Magagnin, E. Valles, J. Electroanal. Chem. 658 (2011) 18–24.
[8] A. Fernández, F.J. Deive, A. Rodríguez, M.S. Álvarez, J. Mol. Liq. 305 (2020) 112824.

[9] D.J. van Osch, L.F. Zubeir, A. van den Bruinhorst, M.A. Rocha, M.C. Kroon, Green Chem. 17 (2015) 4518–4521.
[10] C.W. Zhang, S.Q. Xia, P.S. Ma, Bioresour. Technol. 219 (2016) 1–5.
[11] L. Adhikari, N.E. Larm, G.A. Baker, A.C.S. Sustain, Chem. Eng. 7 (2019) 11036–11043.
[12] A. Fernández, L. González, M.S. Álvarez, F.J. Deive, J. Mol. Liq. 322 (2021) 114960.
[13] B. Nian, C. Cao, Y. Liu, J Chem Technol Biotechnol. 95 (2020) 86–93.
[14] M. Panić, D. Delač, M. Roje, I.R. Redovniković, M.C. Bubalo, Biotechnol. Lett. 41 (2019) 253–262.
[15] C.R. Müller, I. Lavandera, V. Gotor-Fernández, P. Domínguez de María, ChemCatChem 7 (2015) 2654–2659.
[16] E. Durand, J. Lecomte, B. Baréa, E. Dubreucq, R. Lortie, P. Villeneuve, Green Chem. 15 (2013) 2275–2282.
[17] L. Morandeira, M.S. Álvarez, M. Markiewicz, S. Stolte, A. Rodríguez, M.A. Sanromán, F.J. Deive, A.C.S. Sust, Chem. Eng. 239 (2017) 368–377.
[18] J.V. Rodrigues, D. Ruivo, A. Rodríguez, F.J. Deive, J.M.S.S. Esperança, I.M. Marrucho, C.M. Gomes, L.P.N. Rebelo, Green Chem. 16 (2014) 4520–4523.
[19] F.J. Deive, D. Ruivo, J.V. Rodrigues, C.M. Gomes, M.A. Sanromán, L.P.N. Rebelo, J. M.S.S. Esperança, A. Rodríguez, RSC Adv. 5 (2015) 3386–3389.
[20] V.E. Wolf-Márquez, M.A. Martínez-Trujillo, G. Aguilar Osorio, F. Patiño, M.S. Álvarez, A. Rodríguez, M.A. Sanromán, F.J. Deive, Bioresour. Technol. 225 (2017) 326–335.
[21] E. Gutiérrez-Arnillas, M.A. Sanromán, M.A. Longo, A. Rodríguez, F.J. Deive, Sep. Purif. Technol. 248 (2020) 117008.
[22] B. Stuart, Infrared Spectroscopy: Fundamentals and Applications, John Wiley & Sons Ltd, 2004.
[23] J. Coates, Interpretation of infrared spectra, a practical approach, Encyclopedia of, Analytical Chemistry (2000).
[24] N. Delgado-Mellado, M. Larriba, P. Navarro, V. Rigual, M. Ayuso, J. García, F. Rodríguez, J. Mol. Liq. 260 (2018) 37–43.
[25] H. Ghaedi, M. Ayoub, S. Sufian, B. Lal, Y. Uemura, J. Mol. Liq. 242 (2017) 395–403.
[26] M. Kozak, L. Domka, J. Phys. Chem. Solids 65 (2004) 441–445.
[27] S. Zhu, H. Li, W. Zhu, W. Jiang, C. Wang, P. Wu, Q. Zhang, H. Li, J. Mol. Graph. 68 (2016) 158–175.
[28] M. Prekajski, M. Mirković, B. Todorović, A. Matković, M. Marinović-Cincović, J. Luković, B. Matović, J. Eur. Ceram. Soc. 36 (2016) 1293–1298.
[29] J. Hoppe, R. Drozd, E. Byzia, M. Smiglak, Int. J. Biol. Macromol. 136 (2019) 296–304.
[30] C.F. Araujo, J.A.P. Coutinho, M.M. Nolasco, S.F. Parker, P.J.A. Ribeiro-Claro, S. Rudić, B.I.G. Soares, P.D. Vaz, Phys. Chem. Chem. Phys. 19 (2017) 17998.
[31] C. D'Agostino, R.C. Harris, A.P. Abbott, L.F. Gladdena, M.D. Mantle, Phys. Chem. Chem. Phys. 13 (2011) 21383–21391.
[32] T. Khezeli, A. Daneshfar, Ultrason. Sonochem. 38 (2017) 590–597.
[33] I. Delso, C. Lafuente, J. Muñoz-Embid, M. Artal, J. Mol. Liq. 290 (2019) 111236.
[34] Q. Abbas, L. Binder, ECS Trans. 33 (2010) 49–59.
[35] H. Hu, Y. Liu, B. Li, Z. Cui, Z. Zhang, RSC Adv. 5 (2015) 7720–7728.
[36] C. Florindo, F.S. Oliveira, L.P.N. Rebelo, A.M. Fernandes, A.C.S. Sustain, Chem. Eng. 2 (2014) 2416–2425.
[37] F. Heym, B.J.M. Etzold, C. Kern, A. Jess, Phys. Chem. Chem. Phys. 12 (2010) 12089.
[38] W. Chen, Z. Xue, J. Wang, J. Jiang, X. Zhao, T. Mu, Acta Phys-Chim. Sin. 34 (2018) 904–911.
[39] M. Pagliaro, M. Rossi, RSC Green Chemistry Book Series (2008).
[40] Z. Lu, L. Yang, Y. Guo, J. Power Sources 156 (2006) 555–559.
[41] M. Kosmulski, J. Gustafsson, J.B. Rosenholm, Thermochim. Acta 412 (2004) 47–53.
[42] S. Mainberger, M. Kindlein, F. Bezold, E. Elts, M. Minceva, H. Briesen, Mol. Phys. 115 (2017) 1309–1321.
[43] I.M. Aroso, A. Paiva, R.L. Reis, A.R.C. Duarte, J. Mol. Liq. 241 (2017) 654–661.
[44] R.L. Collin, J. Am. Chem. Soc. 79 (1957) 6086.
[45] M. Matsugami, T. Takamuku, T. Otomo, T. Yamaguchi, J. Phys. Chem. B 110 (2006) 12372–12379.
[46] L. Huang, K. Nisinari, J. Polym. Sci. B Polym. Phys. 39 (2001) 496–506.
[47] R.B. Leron, D.S.H. Wong, M.H. Li, Fluid Phase Equilib. 335 (2012) 32–38.
[48] N. Subba, P. Sahu, N. Das, P. Sen, J. Chem. Sci. 133 (2021) 25.
[49] F.J. Deive, M.A. Rivas, A. Rodríguez, J. Chem. Thermodyn. 43 (2011) 487–491.
[50] C. Ortiz, M.L. Ferreira, O. Barbosa, J.C.S. dos Santos, R.C. Rodrigues, Á. Berenguer-Murcia, L.E. Briand, R. Fernandez-Lafuente, Catal Sci. Technol. 9 (2019) 2380–2420.

Synthesis and characterization of a lipase-friendly DES based on cholinium dihydrogen phosphate

María S. Álvarez[a,b*] María A. Longo[a,b], Francisco J. Deive[a,b], Ana Rodríguez[a*]

[a]*Departamento de Ingeniería Química, Universidade de Vigo, 36310, Vigo, Spain*

[b]*CINTECX - Universidade de Vigo, Campus As Lagoas-Marcosende, 36310 Vigo, Spain*

SUPPLEMENTARY INFORMATION

CAPTION TO FIGURES

Fig. S1. Normalized ATR-FTIR spectra at 25 °C for pure components. (A) N_{1112OH}DHP, (B) ethylene glycol, (C) glycerol.

Fig. S2. ^{1}H NMR (400MHz, D_2O) spectra of pure components at 25 °C.

Fig. S3. ^{1}H NMR (400MHz, D_2O) spectra of cholinium dihydrogen phosphate-based DES at 25 °C.

Fig. S4. Thermograms of pure components and DES. (A) N_{1112OH}DHP, (B) Ethylene glycol, (C) Glycerol, (D) DES1, (E) DES2, (F) DES3.

Fig. S5. DSC curves on cooling and heating ramps of pure components and cholinium dihydrogen phosphate-based DES. (A) N_{1112OH}DHP, (B) Ethylene glycol, (C) Glycerol, (D) DES1, (E) DES2, (F) DES3.

Fig. S6. CALB stability evaluation for 24 h spectra at 40 °C in water (blue), ChDHP:EG (2M) (red) and ChCl:EG (2M) (green).

* Corresponding author. *E-mail address:* aroguez@uvigo.es; msaa@uvigo.es

Figure S1

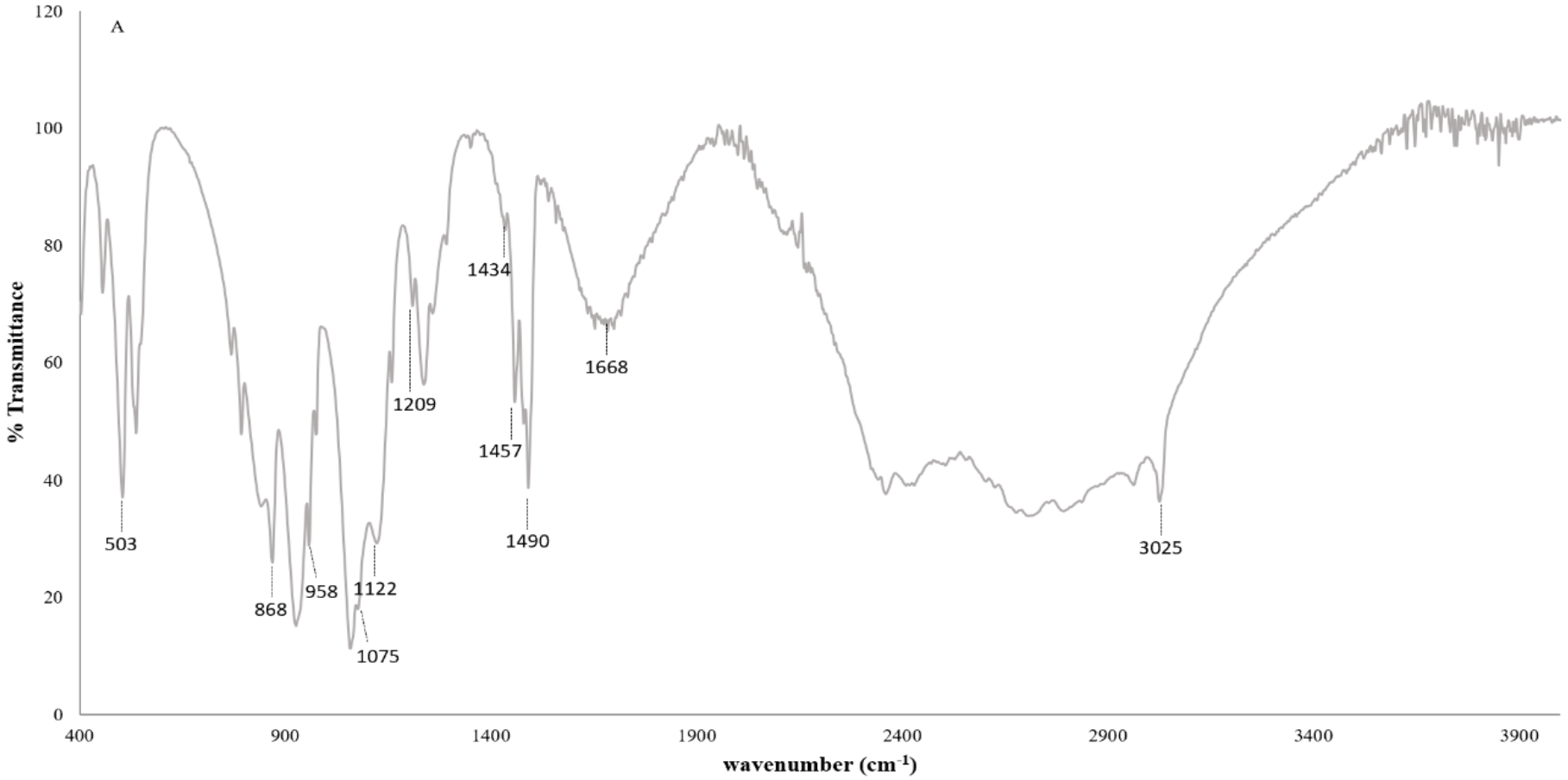
A
% Transmittance
wavenumber (cm-1)
120
100
80
60
40
20
0
400
900
1400
1900
2400
2900
3400
3900
503
868
958
1075
1122
1209
1434
1457
1490
1668
3025

(A)

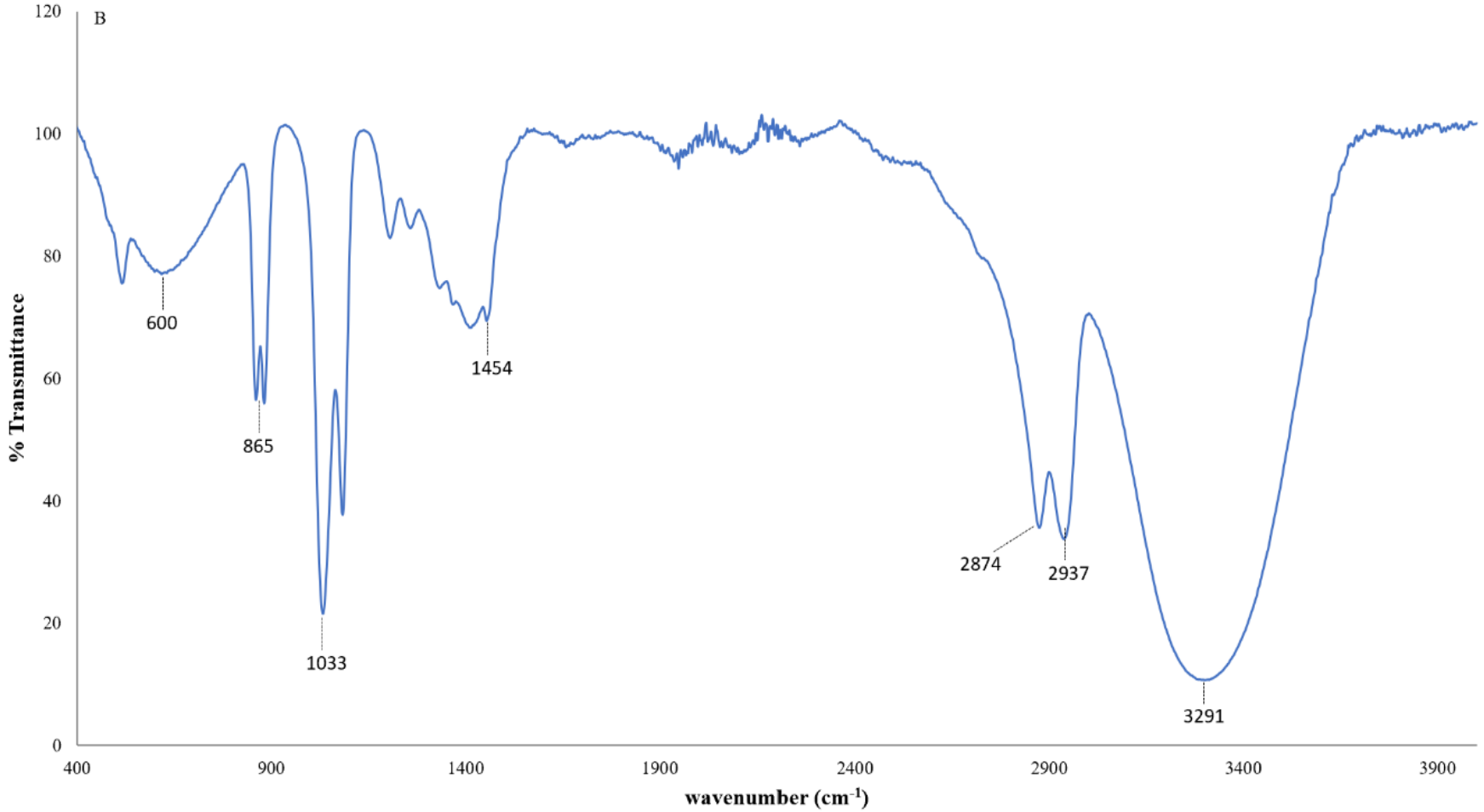
B
120
100
80
60
40
20
0
% Transmittance
600
865
1033
1454
2874
2937
3291
400
900
1400
1900
2400
2900
3400
3900
wavenumber (cm-1)

(B)

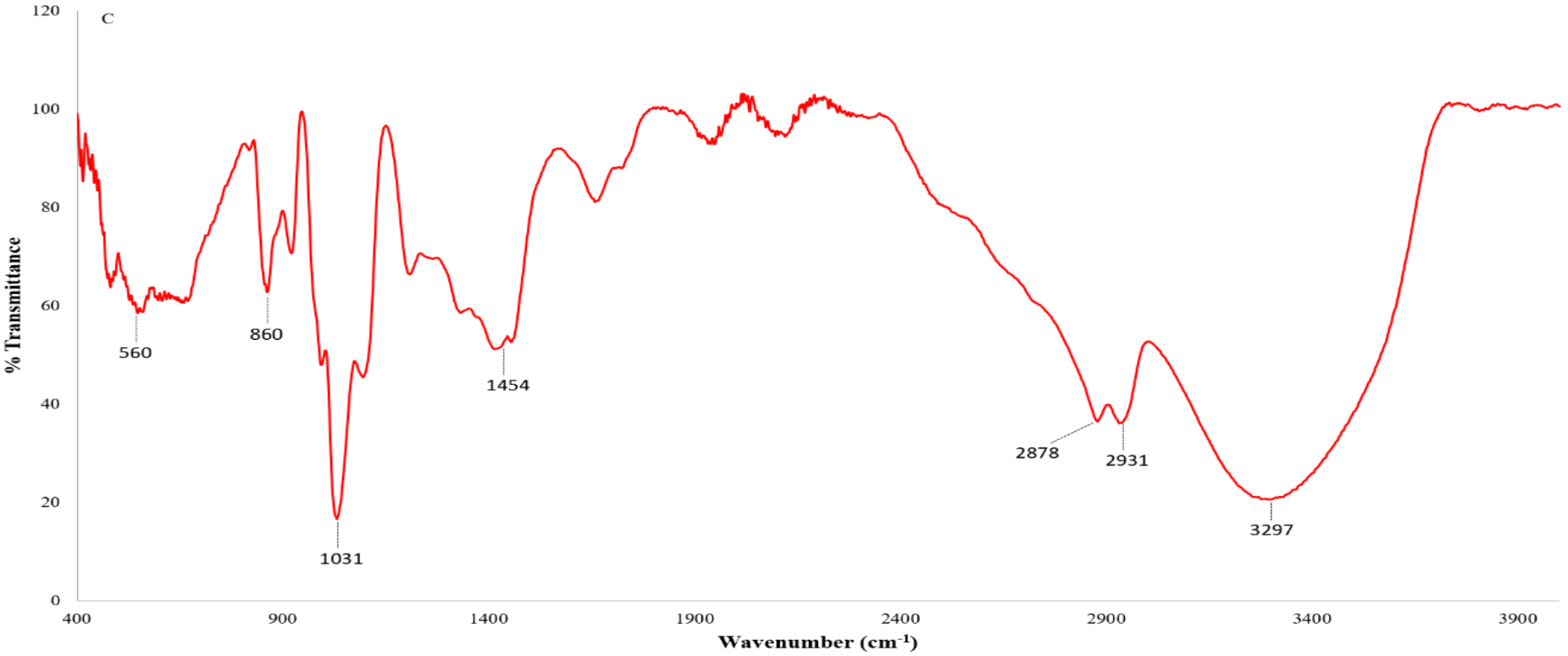
C
120
100
80
60
40
20
0
% Transmittance
560
860
1031
1454
2878
2931
3297
400
900
1400
1900
2400
2900
3400
3900
Wavenumber (cm-1)

(C)

Figure S2

$N_{1112OH}DHP$

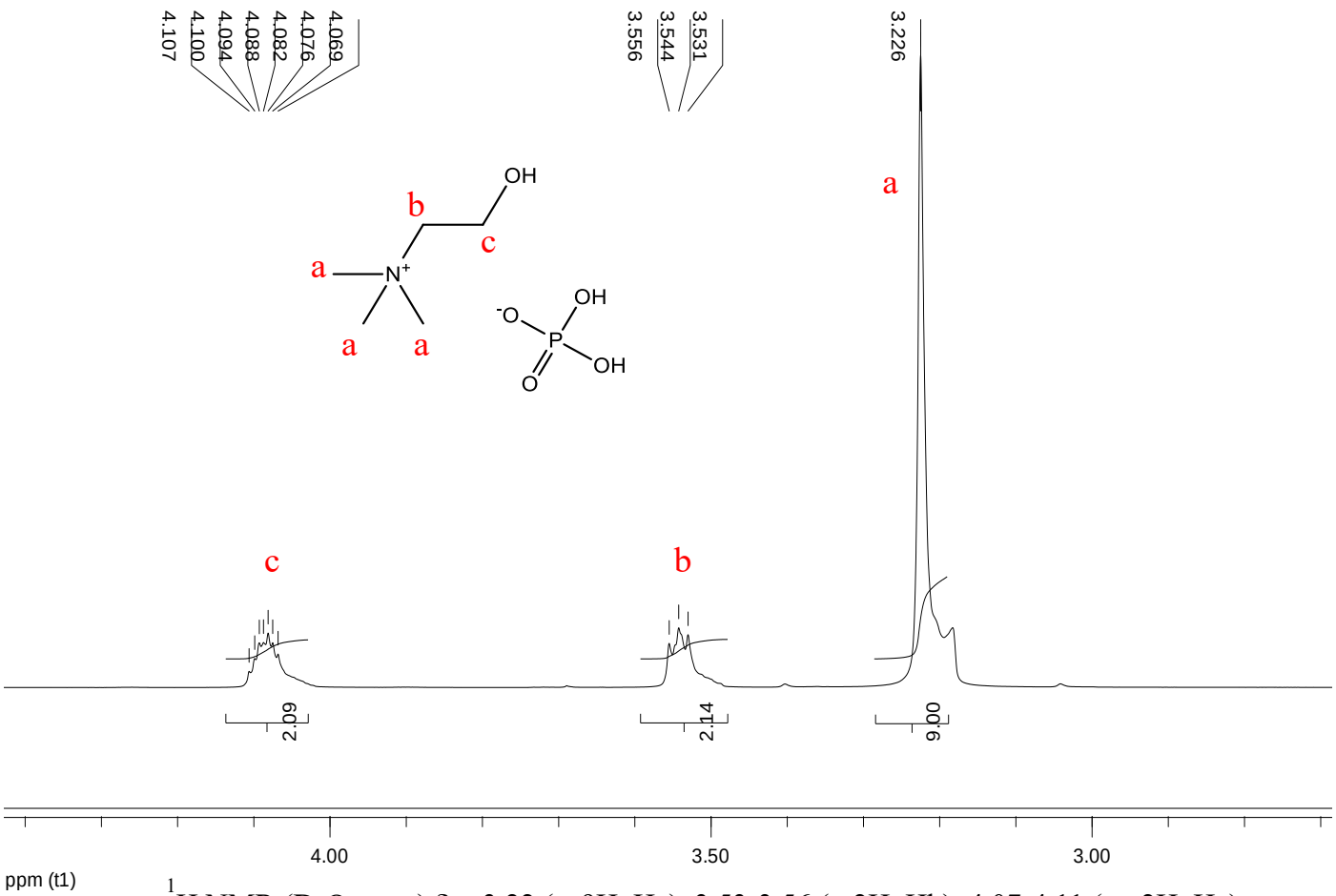

^{1}H NMR (D_2O, ppm) δ = 3.22 (s, 9H, Ha), 3.53-3.56 (t, 2H, Hb), 4.07-4.11 (m, 2H, Hc)

EG

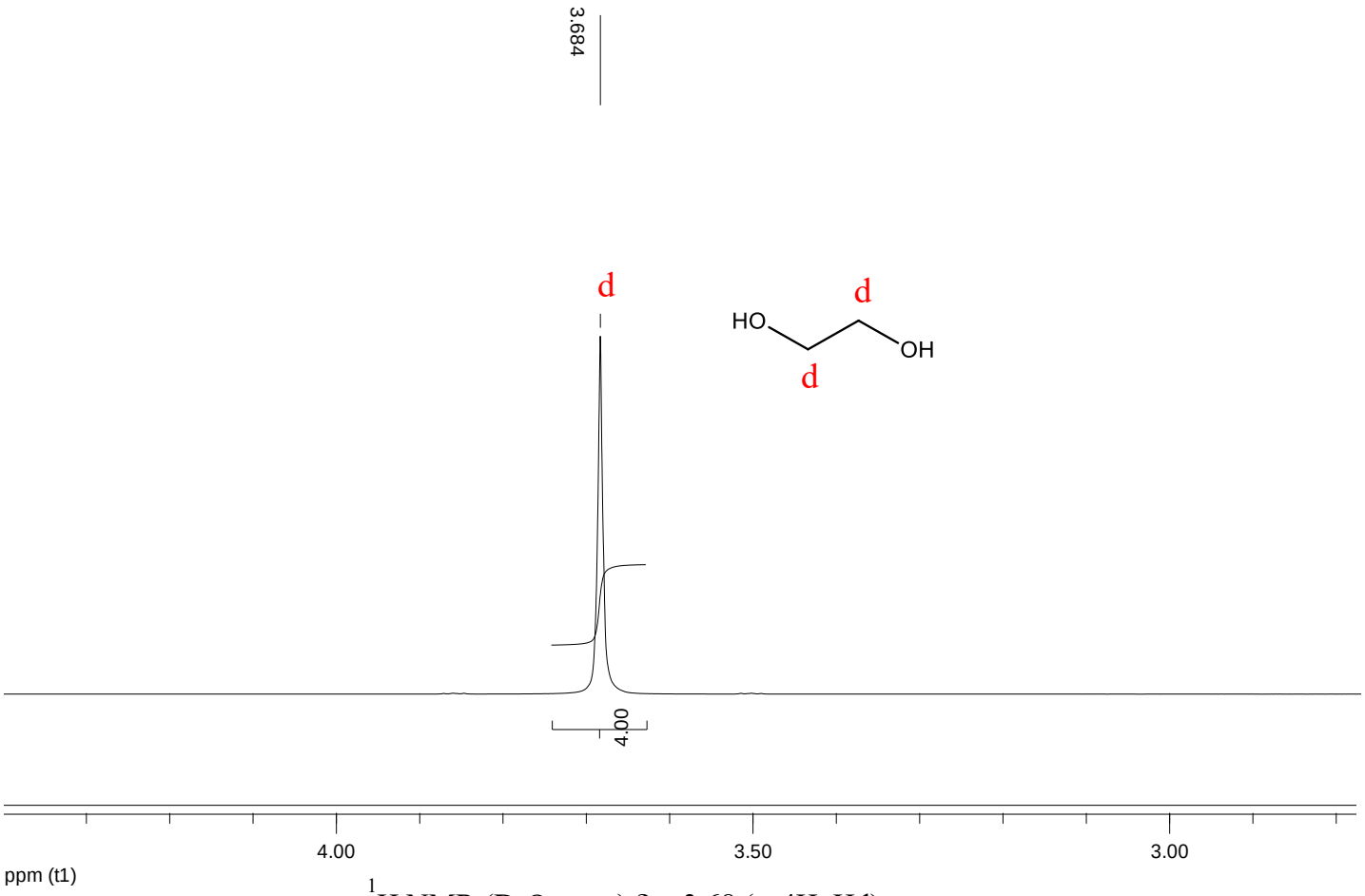

^{1}H NMR (D_2O, ppm) δ = 3.68 (s, 4H, Hd),

GL

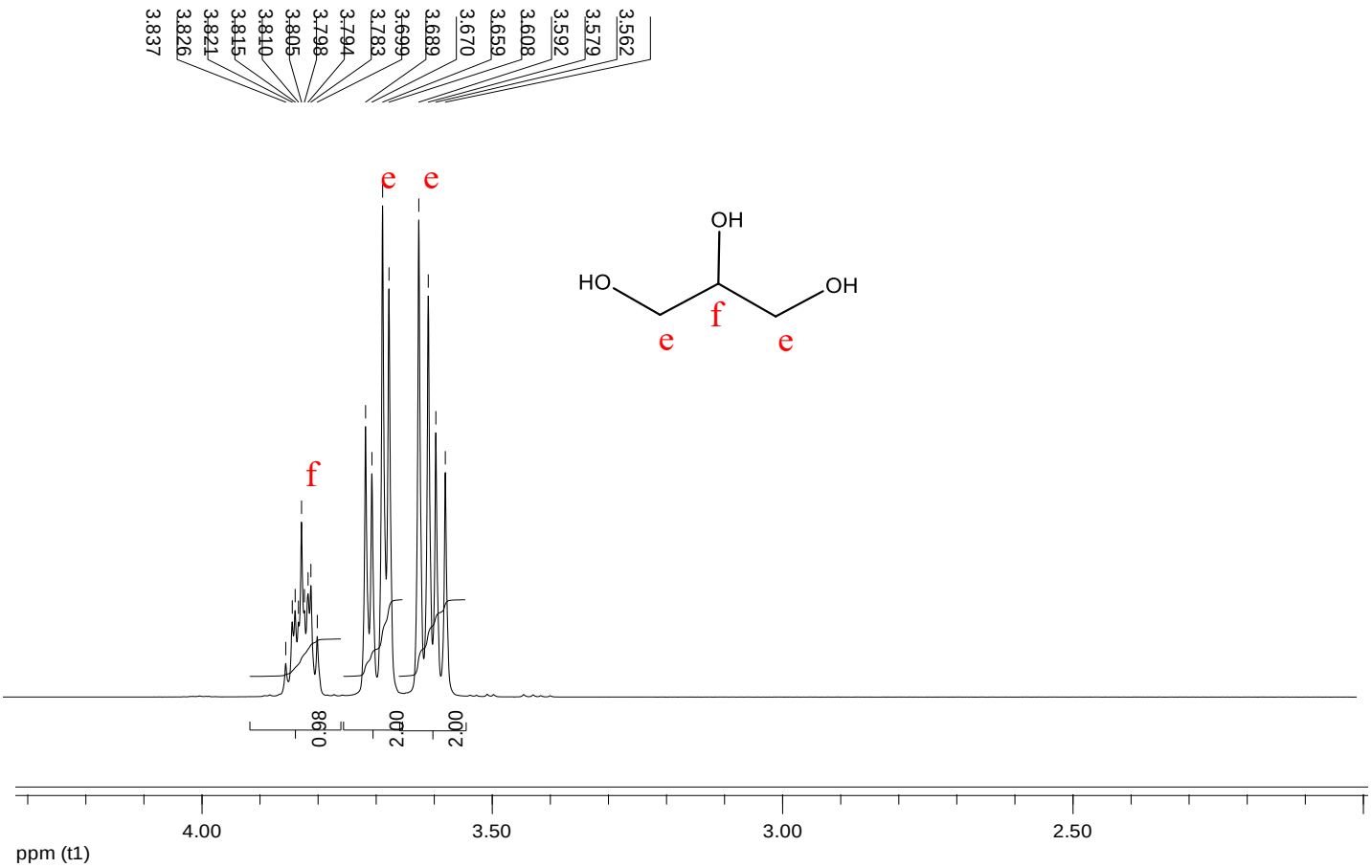

^{1}H NMR (D_2O, ppm) δ = 3.56-3.69 (m, 4H, He), 3.78-3.83 (m, 1H,

Figure S3

DES1 (1:2)

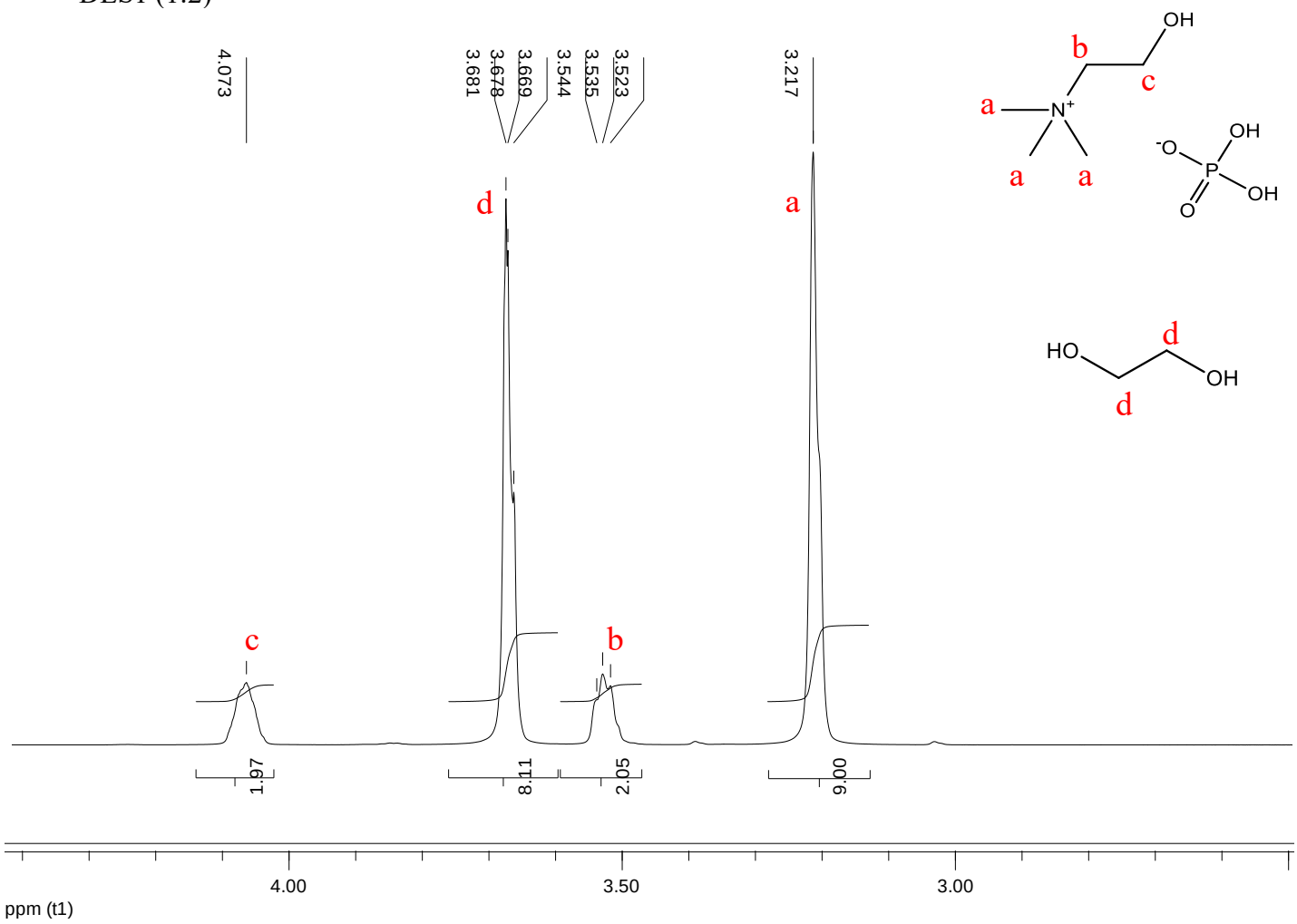

^{1}H NMR (D_2O, ppm) δ = 3.22 (s, 9H, Ha), 3.52-3.54 (t, 2H, Hb), 3.67-3.68 (t, 8H, Hd), 4.07 (s,

DES2 (1:2)

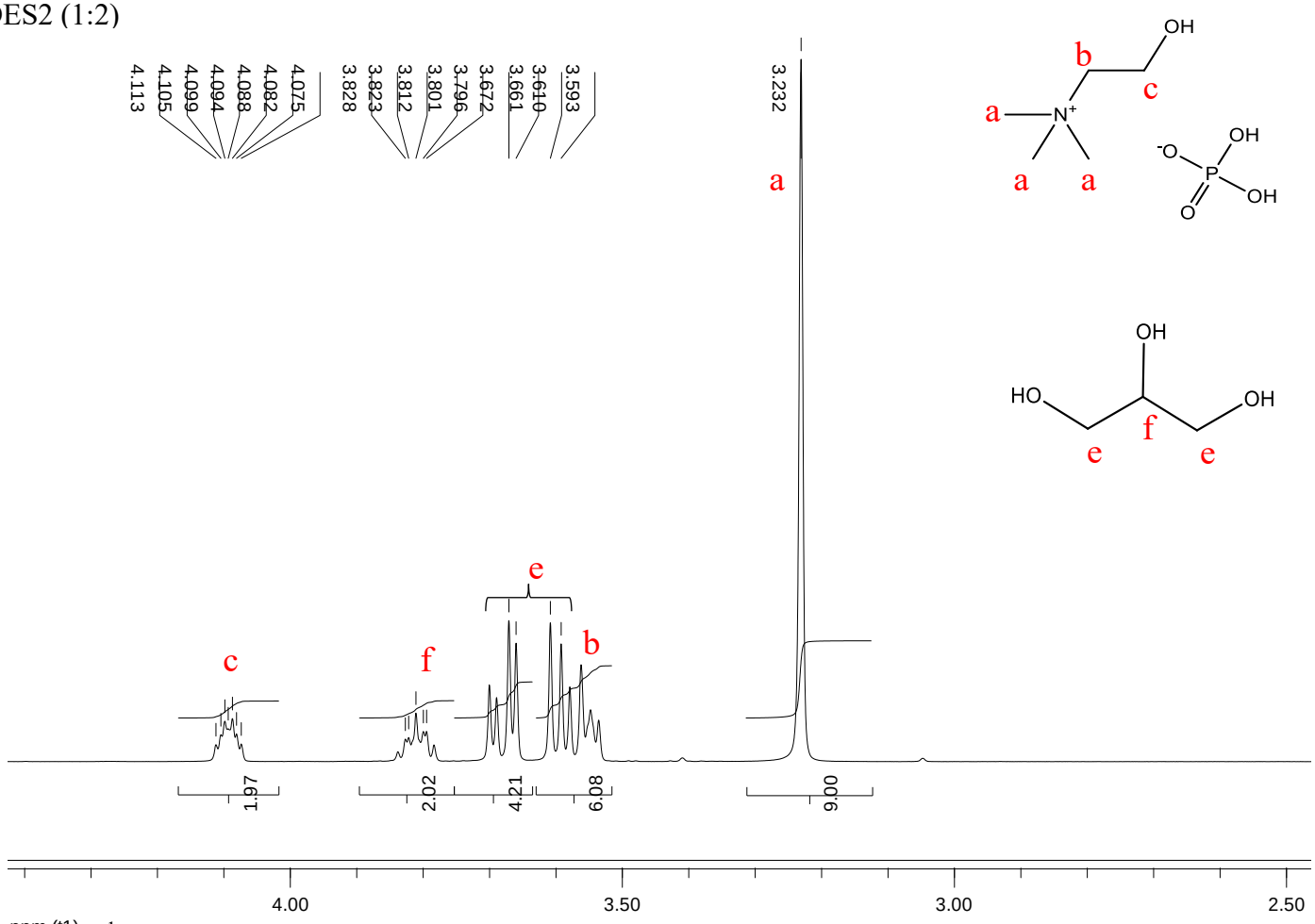

^{1}H NMR (D_2O, ppm) δ = 3.23 (s, 9H, Ha), 3.59-3.67 (2m, 10H, 2Hb and 8He), 3.79-3.83 (m, 2H, Hf), 4.07-4.11 (m, 2H, Hc)

DES3 (1:1:1)

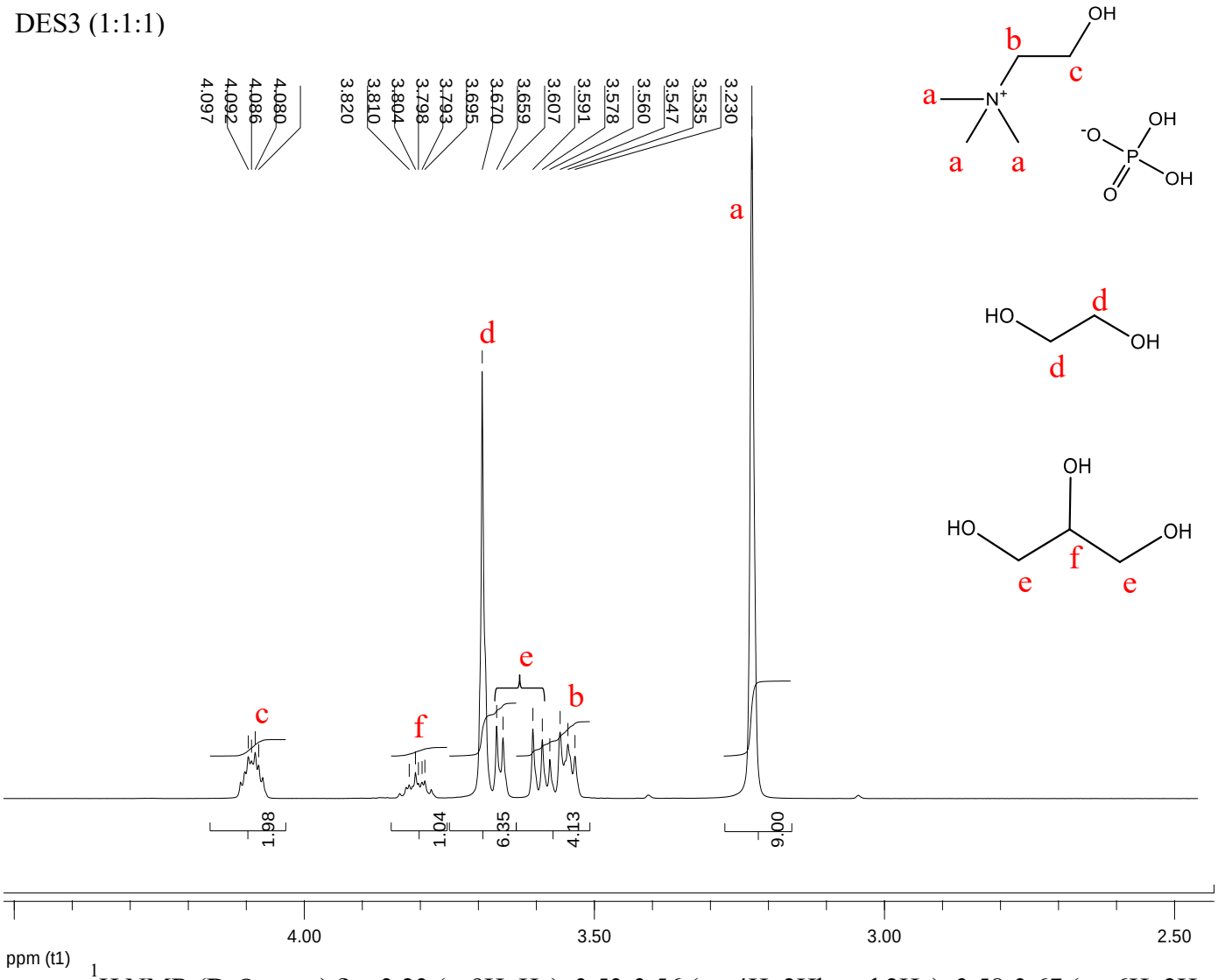

^{1}H NMR (D_2O, ppm) δ = 3.23 (s, 9H, Ha), 3.53-3.56 (m, 4H, 2Hb and 2He), 3.58-3.67 (m, 6H, 2He and 4Hd), 3.79-3.82 (m, 1H, Hf), 4.08-4.10 (q, 2H, Hc)

FIGURE S4

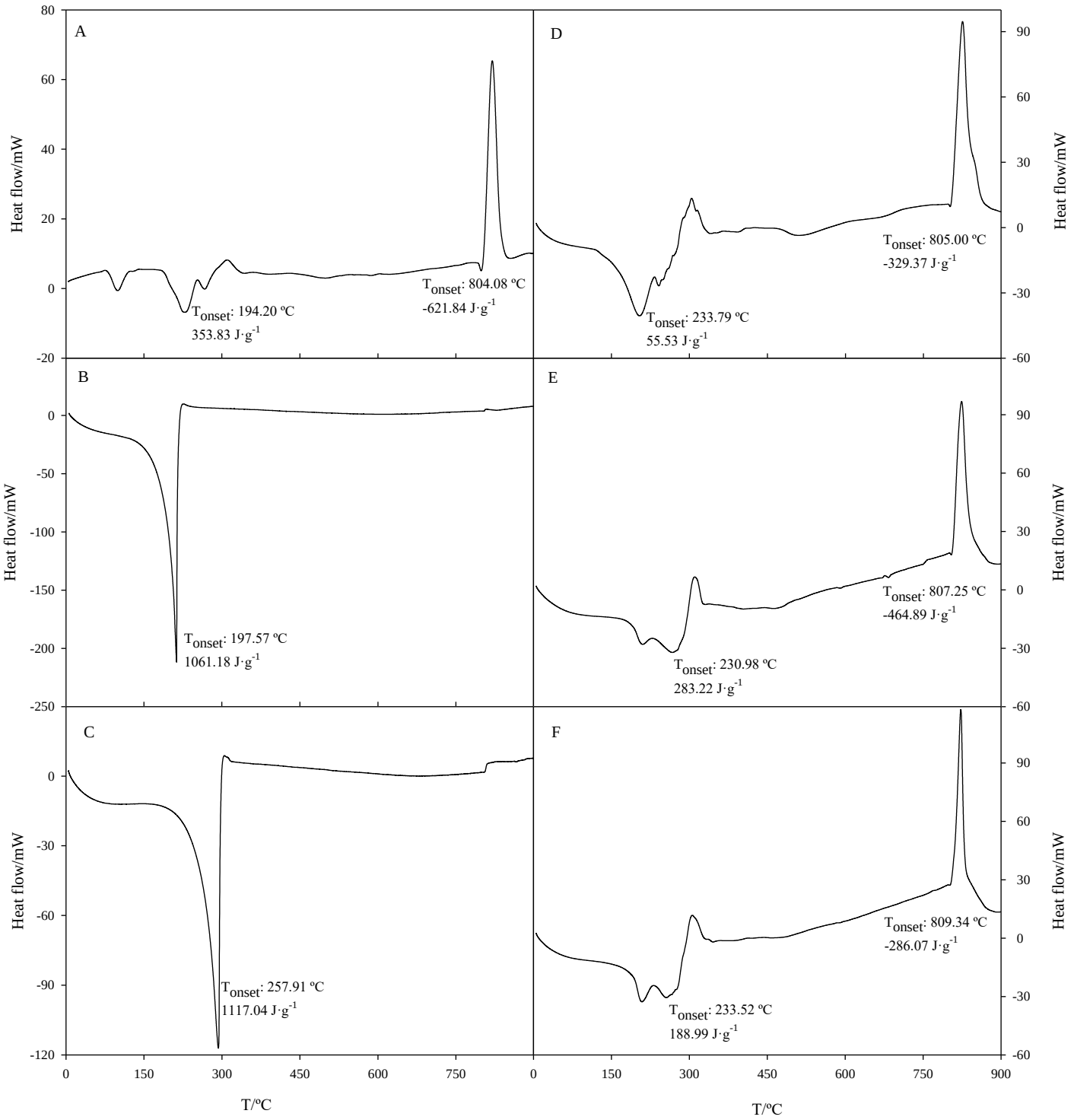
A
Tonset: 194.20 ºC
353.83 J·g-1
Tonset: 804.08 ºC
-621.84 J·g-1
D
Tonset: 233.79 ºC
55.53 J·g-1
Tonset: 805.00 ºC
-329.37 J·g-1
B
Tonset: 197.57 ºC
1061.18 J·g-1
E
Tonset: 230.98 ºC
283.22 J·g-1
Tonset: 807.25 ºC
-464.89 J·g-1
C
Tonset: 257.91 ºC
1117.04 J·g-1
F
Tonset: 233.52 ºC
188.99 J·g-1
Tonset: 809.34 ºC
-286.07 J·g-1
Heat flow/mW
T/ºC

FIGURE S5

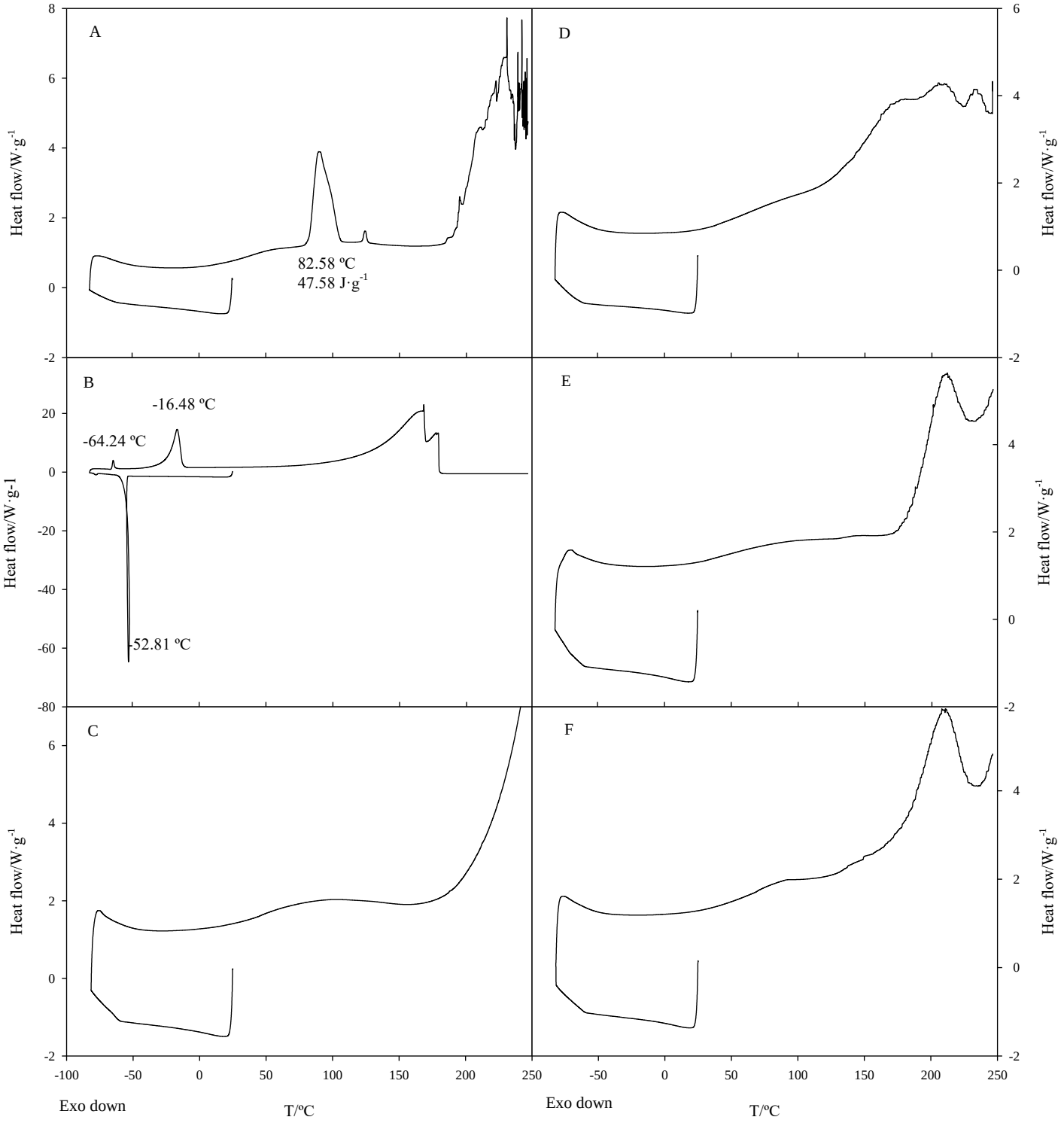
A
82.58 ºC
47.58 J·g-1
D
B
-16.48 ºC
-64.24 ºC
-52.81 ºC
E
C
F
Heat flow/W·g-1
Exo down
T/ºC

FIGURE S6